

# Subseasonal Potential Predictability of Horizontal Water Vapor Transport and Precipitation Extremes in the North Pacific

TIMOTHY B. HIGGINS<sup>a</sup>, ANEESH C. SUBRAMANIAN,<sup>a</sup> WILL E. CHAPMAN,<sup>b</sup>  
DAVID A. LAVERS,<sup>c</sup> AND ANDREW C. WINTERS<sup>a</sup>

<sup>a</sup> *Department of Atmospheric and Oceanic Sciences, University of Colorado Boulder, Boulder, Colorado*

<sup>b</sup> *National Center for Atmospheric Research, Boulder, Colorado*

<sup>c</sup> *European Centre for Medium-Range Weather Forecasting, Reading, United Kingdom*

(Manuscript received 4 October 2023, in final form 8 March 2024, accepted 20 March 2024)

**ABSTRACT:** Accurate forecasts of weather conditions have the potential to mitigate the social and economic damages they cause. To make informed decisions based on forecasts, it is important to determine the extent to which they could be skillful. This study focuses on subseasonal forecasts out to a lead time of four weeks. We examine the differences between the potential predictability, which is computed under the assumption of a “perfect model,” of integrated vapor transport (IVT) and precipitation under extreme conditions in subseasonal forecasts across the northeast Pacific. Our results demonstrate significant forecast skill of extreme IVT and precipitation events (exceeding the 90th percentile) into week 4 for specific areas, particularly when anomalously wet conditions are observed in the true model state. This forecast skill during weeks 3 and 4 is closely associated with a zonal extension of the North Pacific jet. These findings of the source of skillful subseasonal forecasts over the U.S. West Coast could have implications for water management in these regions susceptible to drought and flooding extremes. Additionally, they may offer valuable insights for governments and industries on the U.S. West Coast seeking to make informed decisions based on extended weather prediction.

**SIGNIFICANCE STATEMENT:** The purpose of this study is to understand the differences between the ability to predict high amounts of the transport of water vapor and precipitation over the North Pacific 3 and 4 weeks into the future. The results indicate that differences do exist in a region that is relevant to precipitation on the U.S. West Coast. To physically explain why differences in predictability exist, the relationship between weekly extremes of the extension of the jet stream, IVT, and precipitation over the North Pacific is explored. These findings may impact decisions relevant to water management on the U.S. West Coast susceptible to drought and flooding extremes.

**KEYWORDS:** Atmospheric river; Forecast verification/skill; Hindcasts; Probability forecasts/models/distribution; Seasonal forecasting

## 1. Introduction

Atmospheric Rivers (ARs) are filamentary corridors of water vapor that frequently occur in the warm sector of extratropical cyclones (Neiman et al. 2008). Extreme AR events come with a large cost to society and can result in billions of dollars in damages (Corringham et al. 2019). Integrated vapor transport (IVT) is a key variable that characterizes atmospheric rivers (Shields et al. 2018; Ralph et al. 2019), and it has strong ties to U.S. West Coast precipitation (Waliser and Guan 2017; Ricciotti and Cordeira 2022), particularly when the IVT coincides with orographic lifting in regions of steep topography. Therefore, understanding the predictability of IVT and precipitation can help water resource managers make critical decisions relevant to water supply, droughts, and flooding (Das et al. 2013; Mann and Gleick 2015; Williams et al. 2015). AR and precipitation extremes on the U.S. West Coast are projected to become more severe in the future in both duration and precipitation rate (Dettinger 2011; Curry et al. 2019; Payne et al. 2020; Michaelis et al. 2022). The impacts of a

warming climate on AR extremes will cause the predictability of atmospheric conditions relevant to ARs to be even more critical in the future.

Chaos within the atmosphere causes the predictability of weather at a single instant in time to range from a few days to a few weeks depending on existing circulation patterns and the types of phenomena that are being observed (Lorenz 1965). Weather phenomena on larger spatial scales have higher predictability than phenomena on smaller scales (Jung and Leutbecher 2008). Despite the limit of predictability at singular moments, some processes can create signals in the predictability of weekly averages of conditions that are stronger than the noise of uncertainty caused by chaos. The subseasonal to seasonal (S2S) range is often described to cover forecasts from two weeks to several months into the future (Pendergrass et al. 2020; Robertson et al. 2015; White et al. 2022). Skillful S2S forecasts are typically found to be within “windows of forecast opportunity” that are associated with persistent large-scale oscillation patterns and teleconnections (Robertson et al. 2015; Vitart et al. 2017; White et al. 2017; Mariotti et al. 2020). Barnston and Smith (1996) showed that the El Niño–Southern Oscillation (ENSO) drives seasonal predictability of temperature and precipitation across North America, which results from strong anomalous sea surface

*Corresponding author:* Timothy B. Higgins, timothy.higgins@colorado.edu

DOI: 10.1175/WAF-D-23-0170.1

© 2024 American Meteorological Society. This published article is licensed under the terms of the default AMS reuse license. For information regarding reuse of this content and general copyright information, consult the AMS Copyright Policy ([www.ametsoc.org/PUBSReuseLicenses](http://www.ametsoc.org/PUBSReuseLicenses)).

Brought to you by University of Colorado Libraries | Unauthenticated | Downloaded 05/29/24 10:18 AM UTC

temperatures in the eastern equatorial Pacific that influence the large-scale atmospheric circulation. Palmer (2006) found that predictability over the North Pacific in the extended range is largely dependent on the sign and the amplitude of the Pacific–North American Pattern (PNA), which is characterized by anomalous synoptic-eddy activity in the northeastern Pacific that is frequently initiated by anomalous convection in the tropics (Franzke et al. 2011). Baggett et al. (2017) demonstrated that AR activity can be predicted into weeks 3–5 with some skill depending on activity from the Madden-Julian oscillation (MJO) and the Quasi-Biennial Oscillation. DeFlorio et al. (2019a) showed that AR activity over the North Pacific can change significantly depending on phases of ENSO, the PNA, the MJO, and the Arctic Oscillation. IVT can sometimes provide insight into the prediction of extreme storms farther in advance than precipitation forecasts at medium-range lead times (Lavers et al. 2016). However, there is little known about potential differences between the predictability of IVT and the predictability of precipitation at S2S lead times and their causes. Investigating these differences will demonstrate the value of predicting IVT-related events in future S2S studies.

Physical quantities that are used to describe the state of the atmosphere often have differences in predictability. For instance, temperature typically has higher predictability than precipitation, in part because temperature changes often drive processes that result in precipitation rather than the converse (Koster and Suarez 1995; Luo and Wood 2006). Lavers et al. (2016) demonstrated that IVT has potential predictive skill at longer lead times than precipitation in medium-range forecasts, possibly resulting from the relatively high spatial variability of precipitation and the added possibility for errors to arise from parameterizations that simulate the processes that cause it to occur, such as convection. Errors that occur in simulations of processes that ultimately result in changes to atmospheric conditions contribute to the differences in forecast skill observed between variables. There is still considerable uncertainty concerning differences in predictability between the variables that describe our atmosphere. This study takes a similar approach to Lavers et al. (2016) by utilizing potential predictability. This approach considers the model world and the real world to be identical, which has several benefits. It eliminates model bias entirely, it creates a large sample size, and it is free of spatiotemporal inhomogeneities that characterize an observational framework. While potential predictability is by no means a perfect way to demonstrate real-world relationships, it can still be useful (Kumar et al. 2014).

The frequency of ARs does have skill in S2S forecasts (DeFlorio et al. 2019b) and is often associated with synoptic-scale eddy activity that influences predictability across the western United States. The extreme nature of IVT and precipitation during periods characterized by high and low AR activity, and its subsequent societal impacts, leads us to assess the predictability of the top 10% of extreme IVT and precipitation conditions. Weather regimes with strong negative upper-level geopotential height anomalies just south of Alaska are often associated with anomalously high AR activity over the U.S. West Coast (Amini and Straus 2019). To physically explain the predictability of extreme IVT and precipitation,

we examine the connection of the extreme forecast anomalies to the state and evolution of jet stream regimes over the North Pacific (NPJ) that were shown to have subseasonal predictive skill in Winters (2021). In particular, we examine the extension of the NPJ into the northeastern Pacific, which is largely characterized by strong and frequent extratropical cyclone activity in the region that often plays a critical role in the formation of ARs (Dacre et al. 2015). Previous work (Zhang et al. 2019) showed that 82% of ARs are associated with extratropical cyclones, making the forecast skill of the NPJ highly relevant to the forecast skill of ARs and IVT. Higgins et al. (2000) found that 90th-percentile precipitation events in the Pacific northwest are typically preceded by enhanced tropical convection in the western Pacific and suppressed tropical convection over the Indian Ocean and central tropical Pacific. They show that tropical heating causes convection that can excite wave trains that force anomalously high wind speed extending eastward in the lower midlatitudes of the North Pacific. NPJ regimes can last from several days up to 5 weeks in extreme cases (Winters et al. 2019). The zonal structure of the NPJ allows for a degree of stericity that is not often matched in the chaotic system of the atmosphere at subseasonal scales. During the jet extension, the NPJ can reach the region in which subseasonal skill of extreme IVT anomalies as described in the results section exists.

Below, we show the results of our analysis. In section 2, we describe the reforecasts used for the analysis. In section 3, we discuss the approach toward evaluating subseasonal potential predictability. In section 4, we show the results of our methods. In section 5, we offer a discussion of the results and concluding remarks on our findings.

## 2. Data

In this study, we evaluate potential predictability using a perfect model ensemble framework, wherein each model ensemble acts as a pseudo-observation system. This “perfect model” approach effectively eliminates any potential model bias. Consequently, it enables the authors to assess potential predictability, rather than assessing prediction skill within an ideal modeling system, as demonstrated in prior research (Stockdale et al. 2011).

Reforecasts of IVT and precipitation from the European Centre for Medium-Range Weather Forecasts (ECMWF) Integrated Forecasting System (IFS) were retrieved from the S2S database that is hosted by ECMWF. The data used in this study consist of 11 ensemble members initialized at 0000 UTC, a horizontal grid resolution of  $1.5^\circ \times 1.5^\circ$ , and lead times at 24-h intervals out to 46 days. Output fields of IVT and geopotential height were instantaneous, and fields of precipitation were available for daily (0000–0000 UTC) accumulations. The data span from 1996 to 2015 and use the 2016 IFS model version (Cycle 41r2). Reforecasts within the same season are taken every 3–4 days and initialized during December, January, and February, which typically experience high AR activity on the U.S. West Coast. There are a total of 500 initializations used for reforecasts in this study. IVT and precipitation data from the ECMWF ERA5 reanalysis (Hersbach et al. 2020) was used

to verify relationships between coastal precipitation and IVT in the perfect model space. ERA5 data with a  $0.25^\circ \times 0.25^\circ$  horizontal grid spacing were retrieved each day in December, January, and February from 1996 to 2015.

ARs and precipitation that reach the coastline have the largest impacts on human society. Moore et al. (2021) demonstrated that the state of the NPJ can significantly impact heavy precipitation events along the U.S. West Coast. Winters et al. (2019) used an empirical orthogonal function (EOF) analysis of boreal winter upper tropospheric wind velocity anomalies within the NPJ exit region to define NPJ regimes that describe the state and the evolution of the NPJ. NPJ phases are calculated using the same method as Winters et al. (2019) by projecting instantaneous zonal wind anomalies onto the two leading EOFs of upper-tropospheric zonal wind anomalies between September to May. Other previous studies (Athanasiadis et al. 2010; Jaffe et al. 2011; Griffin and Martin 2017) also found the zonal shift of the jet-exit region to be the leading mode of variability in EOF analyses of upper tropospheric winds over the North Pacific. During jet extension cases, the jet exit region extends toward the U.S. West Coast, bringing large-scale cyclonic flow to the region. The predictability of anomalous IVT within that same region could therefore have downstream impacts at the coast in some cases. EOFs are calculated based on 300 hPa zonal wind anomalies that are defined relative to a 21-day climatological window centered on each analysis time in the Climate Forecast System Reanalysis (CFRS) during 1979–2019. NPJ regimes are subsequently defined using the resultant EOFs. The leading EOF corresponds to an extension and retraction of the jet exit region, and the second leading EOF corresponds to a poleward and equatorward shift of the jet.

### 3. Methods

Both IVT and precipitation forecasts are averaged over 7-day intervals for rolling lead times up to 4 weeks. Data are integrated over time to smooth out high-frequency noise. We use the receiver operating characteristic (ROC) score metric to determine potential predictability (Graham et al. 2010; Kharin and Zwiers 2003; Philippon et al. 2010). The equation used to calculate ROC scores is shown below:

$$A = 1 - \frac{1}{ee'} \sum_{i=1}^e f_i - \frac{1}{2ee'} \sum_{i=1}^e (f'_i - f_i). \quad (1)$$

In the ROC score equation,  $e$  represents the number of events,  $e'$  represents the number of nonevents,  $f_i$  represents the number of nonevents that have a greater forecast probability than the current hit, and  $f'_i$  represents the number of nonevents that have forecast probabilities that are greater than or equal to that of the current hit.

Potential predictability of ROC scores is found by first allowing one ensemble member to function as the “model-observation.” This allows the model to be considered perfect. The perfect model approach was chosen to create a large sample size of data and to avoid model biases. Percentiles in this study are calculated from raw distributions of weekly averaged model data that were valid during December, January, and February of the 20-yr period

in which the forecasts were initialized. Both climatology and percentiles were calculated from model data and were dependent on lead time. When spatial averaging is applied, the percentile threshold is calculated based on spatial averages over the region of interest. IVT and precipitation values that exceed the chosen threshold ( $>90$ th percentile for forecasts of wet conditions) are given a value of one and are considered a “hit” and values outside of the threshold are given a value of zero and considered a “miss.” Computations of ROC scores were made using the ClimPred framework (Brady and Spring 2021). The 90th percentile was chosen as a threshold not only because it is often associated with uncommon and impactful conditions, but also because a percentile requirement at or near the 90th percentile is one of the main defining characteristics of various AR detection algorithms (Brands et al. 2017; Guan and Waliser 2015; Lavers et al. 2012; Mundhenk et al. 2016). The forecast is represented by the percentage of ensemble members in the forecast that exceed the chosen threshold. The ROC score between the 10-ensemble member mean and the “truth” ensemble member is subsequently calculated, and the process is repeated until each of the 11 ensemble members function as the model-observation. All 11 ROC scores are then averaged to attain a single average ROC score corresponding to a selected forecast. Climatological forecasts result in ROC scores around 0.5, which leads us to categorize groups of skillful forecasts as those forecasts that feature ROC scores sufficiently greater than 0.5. A Mann–Whitney  $U$  test is used to assess the significance of ROC scores to determine whether groups of forecasts were skillful overall relative to climatology (Mason and Graham 2002). Significance of ROC scores was assessed at the 95% confidence level.

Coastal precipitation exceeding the 90th percentile was found by first averaging precipitation rate values within the domain bounded by  $32.5^\circ$ – $49^\circ$ N and  $116^\circ$ – $126.5^\circ$ W, over intervals of 7 days. The top 10% wettest weeks are then isolated for further analysis. Precipitation in this region will be referred to as coastal precipitation for the remainder of the study. The IVT anomalies shown during such conditions are found by calculating the mean IVT anomalies over intervals of 7 days. The same process was used to calculate precipitation anomalies, with  $>90$ th-percentile IVT being assessed over  $31.5^\circ$ – $40^\circ$ N,  $139.5^\circ$ – $152.5^\circ$ W. This region will be referred to as the jet exit region for the remainder of the study, as it lies firmly within the area of enhanced flow during jet extension regimes (Winters et al. 2019). The relationship between anomalous weekly coastal precipitation and IVT in the jet exit region is then explored. Understanding this connection serves to verify the relationship between IVT and precipitation in the perfect model space, and to understand the importance of forecasting IVT in the jet exit region. Error bars of differences between ROC scores of forecast IVT and precipitation in the jet exit region were created using a bootstrapping method. Bootstrapping was applied by taking random samples of all pairs of model-observations and forecasts at all points within the jet exit region. 5000 bootstraps were used and each bootstrap consisted of 1000 samples.

Zonal wind anomalies that were projected onto EOF patterns that define aforementioned NPJ regimes from Winters et al. (2019) are calculated relative to the mean of the jet in

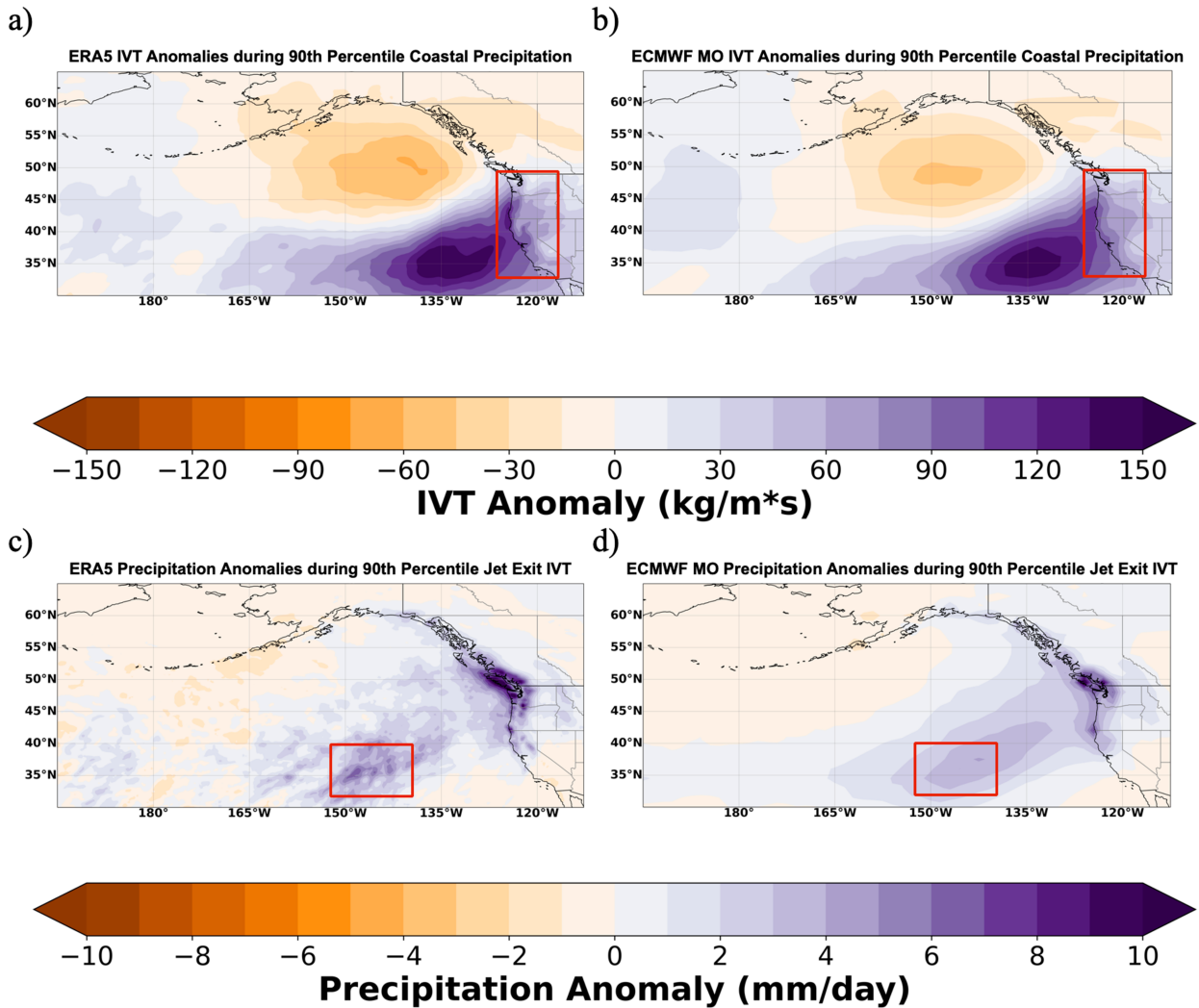


FIG. 1. Composites of IVT anomalies during weeks of >90th-percentile coastal precipitation in (a) ERA5 data and (b) ECMWF model-observed (MO) reforecast data averaged over lead times of 1–7 days. The area that defines locations of coastal precipitation is shown in the red-outlined box. Also shown are composites of existing precipitation anomalies during weeks of >90th-percentile jet exit IVT in (c) ERA5 data and (d) ECMWF MO reforecast data. The area that defines locations of jet exit IVT is shown in the red-outlined box.

ECMWF forecast data. To verify the correspondence between NPJ regimes identified using ECMWF forecast data and reanalysis data, the ensemble mean of PC values at initialization were compared with those derived from both CFSR and ERA-Interim. The correlations of both PC1 and PC2 values are at least 0.99 between all datasets and the greatest mean difference of PC values between any two datasets is 0.07. The % variances ranged from 9.9% to 10.7% for PC1 and from 7.2% to 7.6% for PC2 across all datasets and lead times. There was high consistency overall between the representation of the NPJ regimes in the model and in reanalysis data.

Rossby wave source (RWS) is the rate of change of vorticity due to vortex stretching and vorticity advection from the divergent component of 300 hPa wind velocity [Sardeshmukh and](#)

[Hoskins \(1988\)](#). It is often influenced by tropical heating and causes downstream wave trains in the midlatitudes [Ambrizzi et al. \(1995\)](#). The equation used to calculate RWS is shown below:

$$\text{RWS} = -(\zeta \nabla \cdot \mathbf{v}_x + \mathbf{v}_x \cdot \nabla \zeta). \quad (2)$$

In the RWS equation,  $\zeta$  is absolute vorticity and  $\mathbf{v}_x$  is the divergent component of wind velocity. The inverse Laplacian of the RWS represents the streamfunction, which describes the overall motion of the flow.

#### 4. Results

[Figures 1a](#) and [1b](#) show IVT anomalies during >90th-percentile coastal precipitation. In both the reanalysis space and the perfect

model space, large IVT anomalies exist to the west of the coast, demonstrating the relevance of strong IVT anomalies in the region to downstream precipitation impacts on the coast. The similarities between patterns in ERA5 data and the perfect model space also illustrate that the potential predictability approach represents relationships between precipitation and IVT that are similar to those in a reanalysis, which is constrained by observations.

Precipitation patterns were also explored during weeks of >90th-percentile IVT anomalies in the jet exit region in Figs. 1c and 1d. When >90th-percentile IVT anomalies exist in the jet exit region, downstream positive precipitation anomalies exist on the U.S. West Coast, particularly north of southern California. Differences between the precipitation anomalies in the model space relative to ERA5 are more evident than differences between IVT anomalies in Figs. 1a and 1b. These differences can at least partially be explained by the difference in grid spacing. Precipitation has more spatial variability than IVT does (Figs. 1a,c), making differences in horizontal grid spacing more evident. Differences could not be explained by the additional smoothing added from ensemble members in model-observations, as the result remains similar when a single ensemble member is used instead of the ensemble mean (not shown). Weeks with strong IVT anomalies in the jet exit region are strongly associated with increased downstream precipitation at the coast and the model space can reasonably represent real-world conditions.

Not all conditions can be predicted with equal levels of skill. Estimating potential predictability typically yields lower ROC scores for target conditions of neutral states than they are for above normal and below normal states (Kharin and Zwiers 2003). When the target threshold was set to be within 5% of median IVT and precipitation, neither quantity held any forecast skill at week 3 (not shown). There was no skill in predicting mean conditions anywhere within the evaluation domain at week 3 or week 4. The absence of a strongly anomalous pattern prevents any valuable forecast information from carrying into the subseasonal range. For this reason, there is a limit to what types of conditions can be predicted and in what locations they can be predicted in the subseasonal range.

Predicting both >90th-percentile IVT and precipitation in some regions within the northeast Pacific was skillful out to week 4 using ROC scores (Fig. 2). ROC scores were the highest and remained skillful for the longest duration off the west coast of the United States and Canada. There is large overlap between areas in which IVT and precipitation have forecast skill overall. Differences in ROC scores were minimal on the U.S. West Coast where both forecasts had skill (Fig. 2e). IVT had higher ROC scores than precipitation in both week 3 and week 4 in most areas, with the exception of a region south of Alaska. The area of persistent skill in the southern part of the domain is within a region that experiences frequent impactful AR genesis activity (Prince et al. 2021). This large area of IVT and precipitation forecast skill intersects with the jet exit region (shown in the red box of Fig. 2) and can be heavily influenced by NPJ regimes. Figure 1 demonstrated that strong anomalous IVT near the jet exit region has impacts on downstream precipitation at the coast in both the perfect model space and the real-world.

Figure 3 shows the differences between the predictability of IVT and precipitation in the jet exit region. The mean ROC scores across all points in the jet exit region were higher for predicting >90th-percentile IVT than they were for >90th-percentile precipitation. While a clear majority of samples of IVT forecasts were more skillful than precipitation forecasts at week 3 and week 4, the error bars did extend past the point of IVT having greater skill. This indicates that subseasonal IVT forecasts are not more skillful than subseasonal precipitation forecasts in the jet exit region in all cases. However, the difference in mean ROC scores was significant at the 95% level when a Student's *t* test was applied to the synthetic data. The ROC score of IVT was higher than the ROC score of precipitation in 89% of cases, which provides statistical evidence that the IVT does have more skill at these lead times.

ROC scores in the jet exit region were calculated at all lead times up to 4 weeks in Fig. 4. The impact of the sharp spatial gradients associated with precipitation on predictability was investigated by applying spatial averaging. Spatial averaging was applied by taking the spatial mean of both quantities over the jet exit region before calculating ROC scores (Fig. 4b) rather than by calculating ROC scores at each point in the region first before taking the mean (Fig. 4a). The result of spatial averaging leading to higher predictability is consistent with results presented in Luo and Wood (2006). When spatial averaging was not applied, IVT had more forecast skill than precipitation at every lead time and the difference was always significant at the 95% confidence level (Fig. 4a). After spatial averaging was applied, mean IVT ROC scores were still higher than mean precipitation ROC scores, but the gap closed considerably. Differences in ROC scores remained significant at most lead times, particularly in the subseasonal range. The remaining differences after spatial averaging indicate that sharp spatial gradients of precipitation cannot fully explain differences in predictability in the subseasonal range.

A principal component analysis (Winters et al. 2019) is used to track the state and evolution of the NPJ during forecasts of wet weeks when wet conditions exist in model-observations at week 4 (Fig. 5). A jet extension signal exists when both >90th-percentile IVT and precipitation exist in model-observations. The jet extension was stronger during >90th-percentile IVT than it was during >90th-percentile precipitation. The signal from the NPJ was also evaluated when individual forecasts of wet weeks were skillful in comparison with being unskillful. Skillful forecasts are those in which at least 2 of the 10 ensemble members predict the >90th-percentile threshold of IVT or precipitation to be a "hit" when a "hit" is model-observed. Since >90th-percentile conditions occur during 10% of weeks, a climatological forecast would predict it to occur in 1 of 10 ensemble members and is considered to be unskillful. When wet weeks of both IVT and precipitation were model-observed, there was a stronger jet extension model-observed during skillful forecasts than during unskillful forecasts. The result was significant at the 95% level using a Student's *t* test for both IVT and precipitation at both week 3 and week 4. Precipitation forecasts that were not skillful had little to no relationship with the NPJ, indicating that the presence of a jet extension regime may contribute to skillful forecasts of >90th-percentile

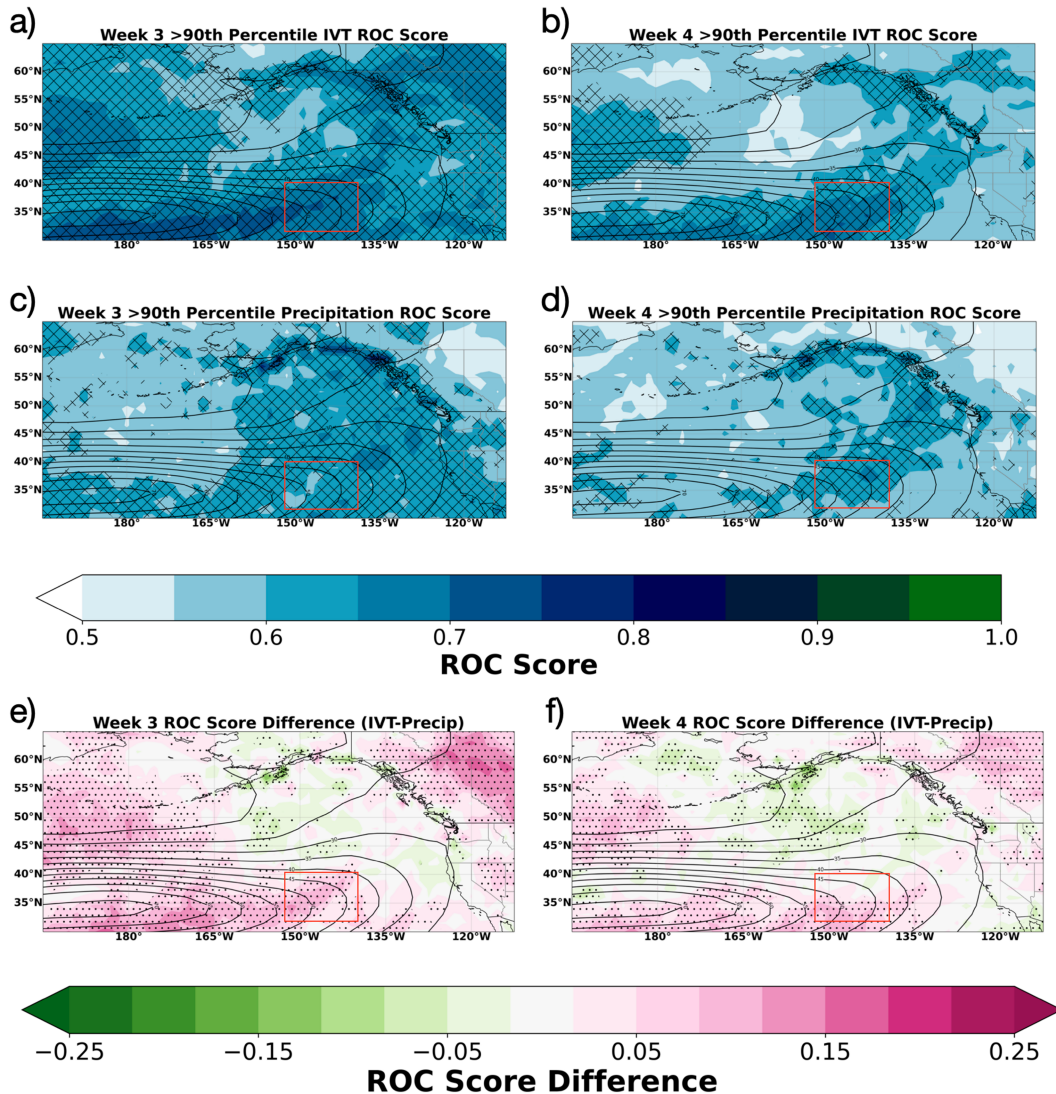


FIG. 2. ROC scores (shaded) of >90th-percentile (a),(b) IVT and (c),(d) precipitation at (left) week 3 and (right) week 4. A Mann–Whitney  $U$ -test was used to demonstrate locations in which the ROC scores were high enough to be considered skillful (hatched areas). Differences in ROC scores are shown at (e) week-3 and (f) week-4 lead times. Stippling shows significance of differences using a two-sided Student’s  $t$  test. Unshaded contours represent model-observed climatology of 300-hPa wind speed ( $\text{m s}^{-1}$ ) with increments of  $5 \text{ m s}^{-1}$  during >90th-percentile jet extension regimes. The red-outlined box represents the jet exit region.

jet exit precipitation in the subseasonal range (Figs. 5a,c). Subseasonal forecasts that were skillful had stronger responses from the NPJ than those that were not skillful overall.

In addition to understanding model-observed conditions of the NPJ during skillful and unskillful forecasts of wet weeks, conditions of IVT and precipitation were also model-observed during skillful and unskillful forecasts of the NPJ (Fig. 6). Skillful individual forecasts are once again forecasts in which at least two ensemble members predict >90th-percentile conditions when >90th-percentile conditions are model-observed. This approach demonstrates the impact of the predictability of the jet on anomalies of IVT and precipitation. Rather than considering >90th-percentile IVT or precipitation as a “hit,”

>90th-percentile PC1 values of the NPJ are used instead to understand model-observed conditions during strong jet extensions. The result of applying this process is shown in Fig. 6. During model-observed >90th-percentile jet extensions, positive IVT anomalies extended eastward toward the coast. Model-observed IVT anomalies were stronger slightly east of the jet exit region during skillful forecasts of the NPJ (Figs. 6e,f) and a significant model-observed positive precipitation anomaly existed on the coast of northern California (Figs. 6a,b). A significant negative precipitation anomaly existed in the Pacific Northwest during unskillful jet extension forecasts at week 4 (Fig. 6d). This result demonstrates that forecasts of strong jet extensions in the S2S range can provide

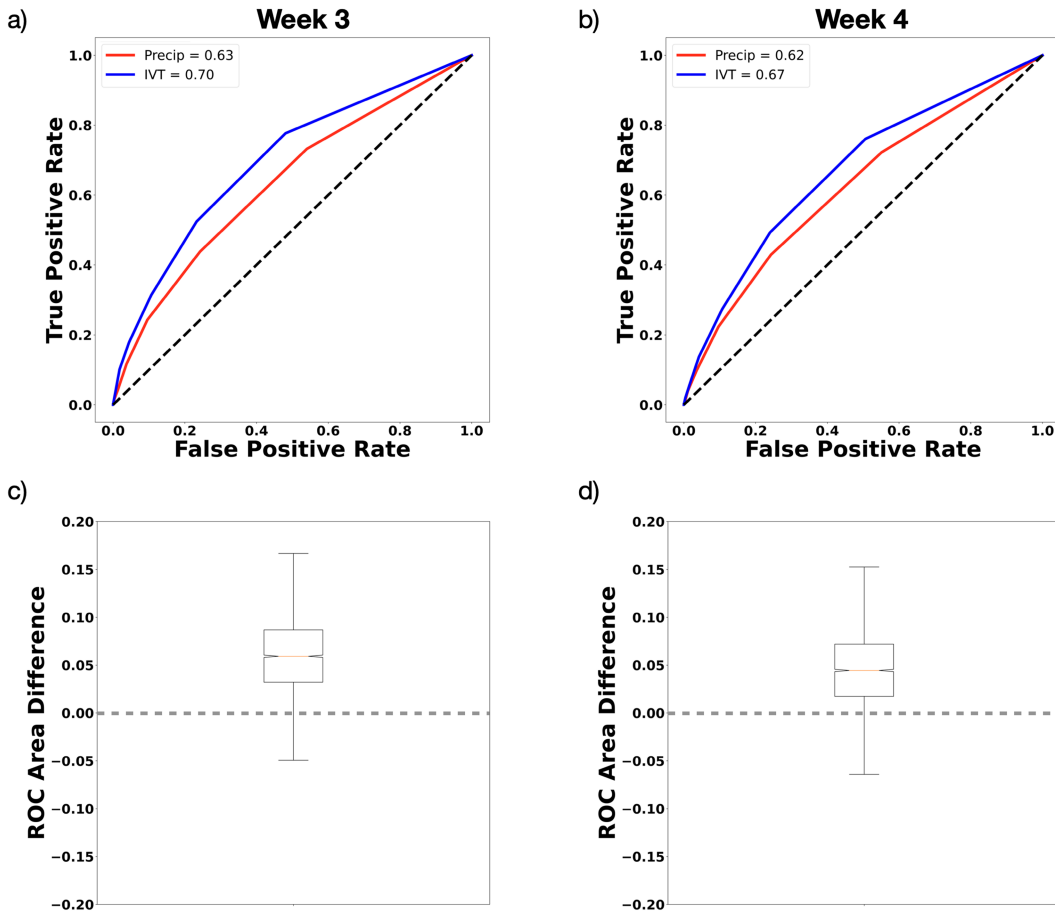


FIG. 3. Mean ROC scores of IVT and precipitation in the jet exit region are also shown at lead times of (a) 3 and (b) 4 weeks. Five thousand bootstraps were used to generate error bars for differences in ROC scores in the jet exit region at lead times of (c) 3 and (d) 4 weeks. Each bootstrap used 1000 samples. Differences are calculated by subtracting precipitation ROC scores from IVT ROC scores.

information relevant to downstream impacts on the coast. Recall that Fig. 5 showed that high forecast skill of >90th-percentile IVT in the jet exit region was also tied to strong jet extension regimes. Therefore, a strong downstream signal of positive

precipitation anomalies during high-skill forecasts of strong jet extension regimes suggests that such anomalies may be dynamically linked to exceptionally strong jet extension regimes.

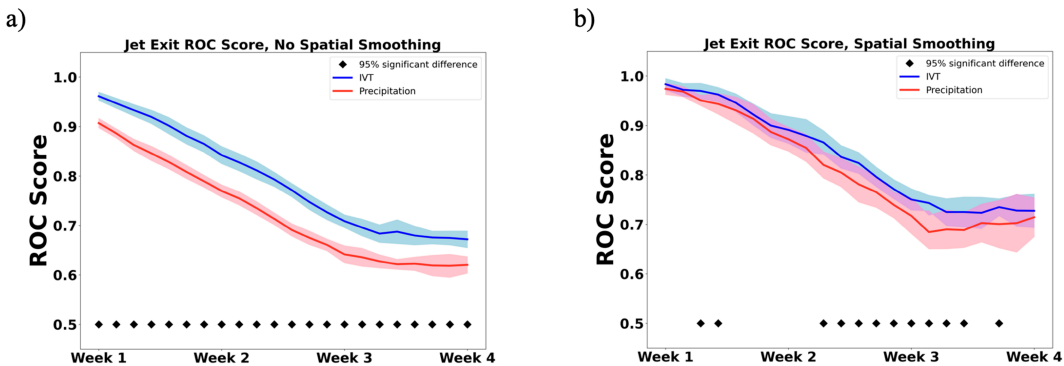


FIG. 4. Mean ROC scores of precipitation and IVT in the jet exit region at all lead times up to 4 weeks. Spatial averaging (a) was not applied and (b) was applied. A Student's *t* test was used to assess statistical significance at the 95% level at all lead times. The shaded area represents one standard deviation above and below the mean.

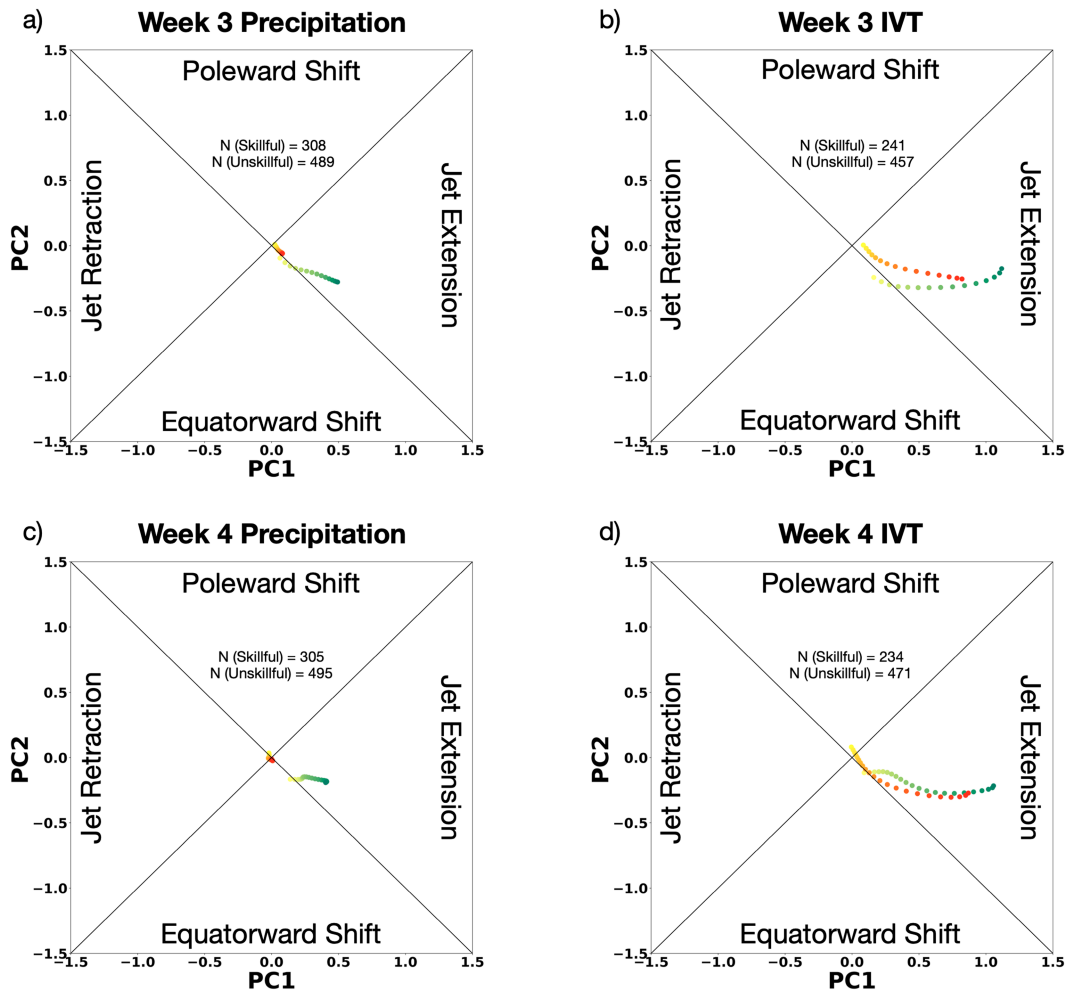


FIG. 5. Composites of principal component analysis values of the model-observed NPJ during model-observed (a) >90th-percentile precipitation at week 3, (b) >90th-percentile IVT at week 3, (c) >90th-percentile precipitation at week 4, and (d) >90th-percentile IVT at week 4 during skillful (green) and unskillful (red) forecasts. Lighter colors represent earlier lead times and become darker through the progression of the forecasts. Forecasts of wet weeks within all individual points from 31.5° to 40°N and from 139.5° to 152.5°W were used. Each data point represents a mean of lead times spanning 7 days starting at days 1–7. The  $N$  (Skillful) and  $N$  (Unskillful) values represent the number of unique initialization times in which model-observed >90th-percentile conditions existed during skillful and unskillful forecasts, respectively.

Composites of forecasts of geopotential height at both 850 and 300 hPa were calculated during cases of model-observed >90th-percentile IVT at week 4 in the jet exit region (Fig. 7). The result illustrates anomalous activity in the forecast when high amounts of IVT are model-observed. Negative geopotential height anomalies at both levels were forecast from week 1 and strengthened out to week 4. The center of the anomalies appeared slightly south of Alaska and shifted toward the southwest afterward. The location of the forecast anomalies at both levels remained somewhat consistent with each other, with the upper-level anomalies lying slightly west of their lower-level counterparts, indicative of an environment favoring surface cyclogenesis. The resulting surface cyclones produce strong westerly geostrophic winds near the jet exit region, which directly impacts IVT. The forecasts of

geopotential height during strong model-observed jet exit IVT show a clear signal of anomalous flow toward the jet exit region in the subseasonal range.

In Fig. 8, standardized ensemble spread of 300-hPa geopotential height with respect to climatology is shown during skillful forecasts of IVT in the jet exit region. When unskillful forecasts were used, the pattern resembled the climatological spread (not shown). When IVT is skillfully forecast in the jet exit region, anomalously high ensemble spread exists near the eastern edge of the negative geopotential height anomaly over the North Pacific. This area has frequent overlap with locations in which ROC scores over the North Pacific were the lowest for both precipitation and IVT (Fig. 2). The anomalously high spread has a weaker presence near the jet exit region. Anomalously low spread occurs upstream of the forecast

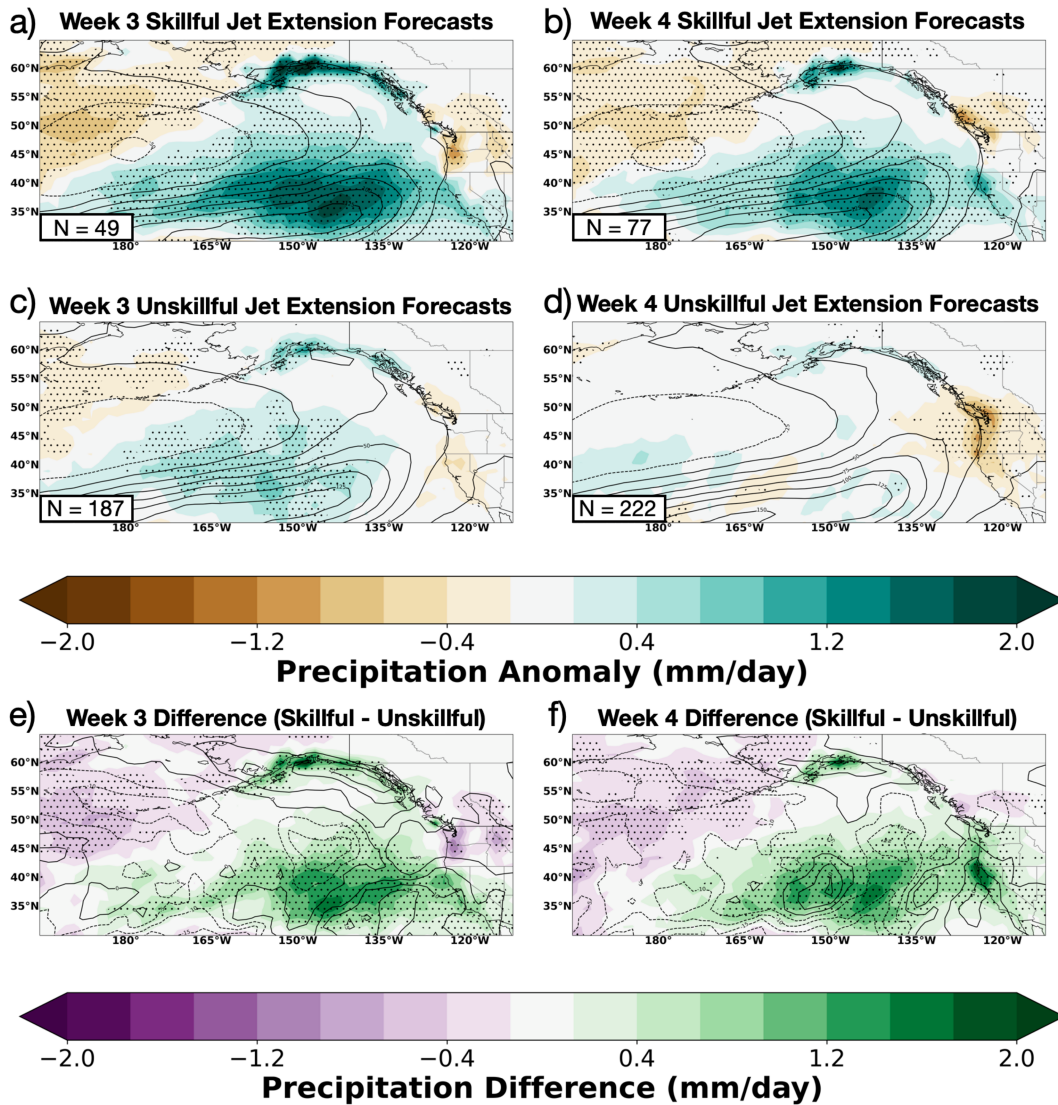


FIG. 6. Composite maps of model-observed anomalies of precipitation (shaded) and IVT (contours) during (a) skillful forecasts and (c) unskillful forecasts of >90th-percentile PC1 values of the jet extension regime at week 3. Composite maps of model-observed anomalies (calculated from data within the model) of precipitation and IVT are also shown during (b) skillful and (d) unskillful forecasts at week 4. Stippling indicates areas in which anomalies of precipitation are significant at the 95% confidence level using a Student's *t* test. Composite maps of the differences between conditions during skillful and unskillful forecasts are also shown at lead times of (e) 3 and (f) 4 weeks. Stippling indicates areas in which differences of precipitation are significant at the 95% confidence level using a Student's *t* test. Sample size in (a)–(d) represents the number of unique initialization times in which model-observed >90th PC1 conditions existed.

negative geopotential height anomaly and in the tropical western Pacific. The region upstream of negative geopotential height anomalies has been shown to experience persistent extratropical cyclone development. Forecast RWS anomalies (Figs. 8c,d) are also shown during skillful forecasts at lead times of 3 weeks and 4 weeks. The RWS was anomalously high over much of east Asia and anomalously low over much of the northeast Pacific. Similarly, taking the inverse Laplacian of the RWS indicated that much of the wave activity downstream occurred within or close to the jet exit region. Patterns

of ensemble spread, forecast geopotential height anomalies, forecast anomalous RWS, and the inverse Laplacian of forecast RWS remained consistent between lead times of 3 weeks and 4 weeks.

### 5. Conclusions

This study explored the potential predictability of S2S forecasts of IVT and precipitation. The results show that predicting strong positive IVT and precipitation anomalies can be

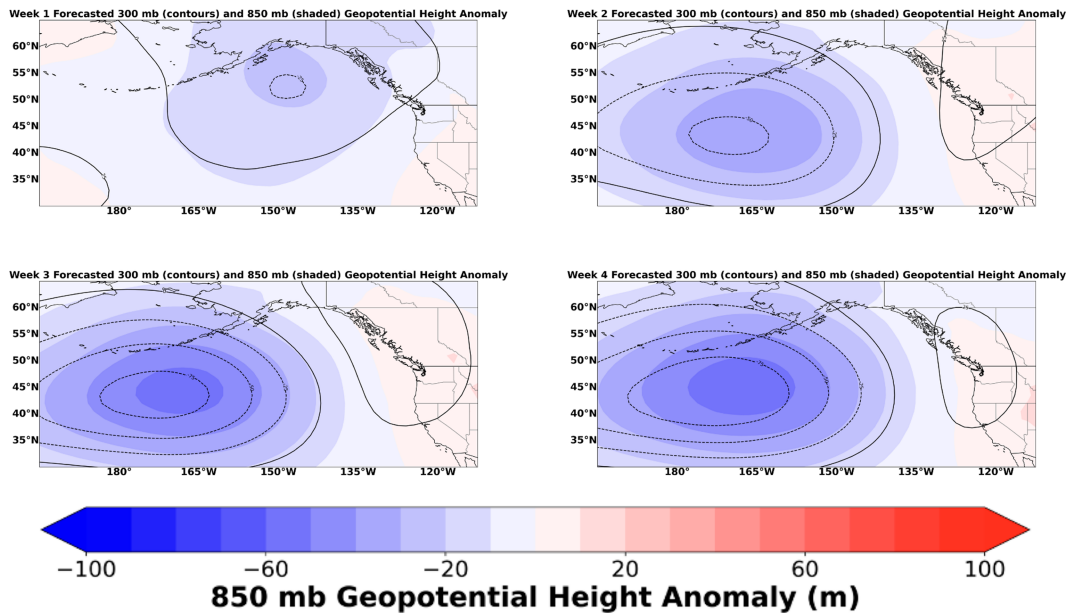


FIG. 7. Mean composites of forecast anomalies of geopotential height at 850 (shaded) and 300 (contours) hPa conditioned on >90th-percentile model-observed IVT occurring at a week-4 lead time. The same set of forecasts are used for each panel, with each composite differing by lead time; for example, the top-left panel is a composite of the forecasts 3 weeks prior to the bottom-right panel.

skillful in some areas across the Northeast Pacific out to week 4. Predicting high IVT, which is the primary characteristic used to define and describe atmospheric rivers, was generally more skillful over a larger area relative to predictions of high precipitation. A possible explanation for this could relate to the connection between IVT and the NPJ. Throughout medium-range lead times, the difference in forecast skill between IVT and precipitation forecasts shown in previous work (Lavers et al. 2014) appears to be partially caused by the influence of subsynoptic or mesoscale features on the predictability of precipitation, whereas the predictability of IVT is more closely related to synoptic-scale features. During skillful 4-week forecasts of >90th-percentile IVT and precipitation shown in this work, local variability became less relevant to the gap in forecast skill at subseasonal lead times and the gap in forecast skill between IVT and precipitation appears to be more closely related to a specific synoptic scale teleconnection associated with the NPJ. It must be noted that while ROC scores of IVT are higher on average in the jet exit region and that the difference in means relative to precipitation forecasts is significant, there can still be individual cases in which the precipitation forecasts have higher ROC scores. This result could be explained by the chaos of our climate system, which allows some cases to deviate from the relationship described above.

Figure 5 demonstrated that jet extension regimes are more strongly correlated with strong IVT anomalies than they are to high precipitation anomalies. Forecasts that were skillful were also associated with a stronger zonal extension of the jet. While the jet extension regime was stronger when forecasts of IVT were skillful, it must be noted that it was still present when forecasts of IVT were not skillful. The predictability of

jet extension regimes into week 4 across a number of S2S models shown by Winters (2021) could explain the predictability of anomalously high IVT that is often associated with those regimes. Persistence of such IVT conditions can often be associated with “AR families” that occur during jet extension-like patterns (Fish et al. 2019). The existence of such a skillful teleconnection that can strongly influence the predictability of IVT could explain much of the gap between the predictability of IVT and the predictability of precipitation in the subseasonal range. Differences in errors resulting from parameterized processes also lead to precipitation errors and uncertainty in horizontal mass convergence (Lavers et al. 2014).

Significant precipitation anomalies were also found on the west coast of North America when jet extensions were model-observed to be strong (exceeding the 90th percentile). There is a significant positive precipitation anomaly in northern California during skillful forecasts of jet extensions and a negative precipitation anomaly during unskillful forecasts of jet extensions. During skillful jet extension forecasts, a negative precipitation anomaly exists over the coast of British Columbia. When the forecasts had skill, IVT was stronger in the jet exit region while it was weaker east and west of this region at a week-4 lead time. This pattern suggests an accelerated breakdown of synoptic eddies in the region when forecasts did not have skill. When synoptic eddies dissipate before reaching the jet exit region, the NPJ is limited from extending farther east toward the coast and both IVT and precipitation across the eastern Pacific are limited from having forecast skill beyond that point.

Skillful jet extension forecasts often occurred when the jet extension regime was stronger and existed to some degree

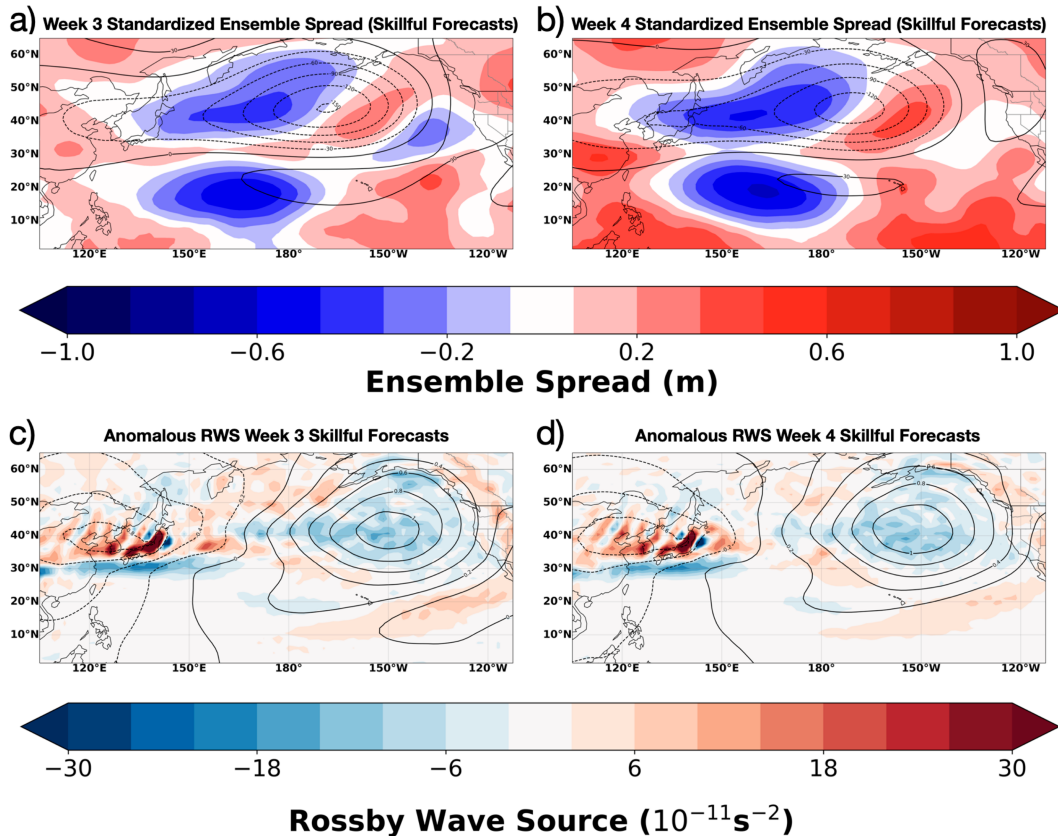


FIG. 8. Conditions during skillful forecasts of IVT in the jet exit region. Standardized ensemble spread (shaded) of geopotential height at 300 hPa during skillful forecasts at lead times of (a) 3 and (b) 4 weeks is shown. Forecasts of 300-hPa geopotential height anomalies during skillful forecasts are shown with line contours separated by 30 m. Also shown are composites of anomalous Rossby wave source (shaded) at lead times of (c) 3 and (d) 4 weeks during skillful forecasts. The inverse Laplacian of the Rossby wave source composites is shown by line contours with increments of  $0.2 \text{ m}^2 \text{ s}^{-2}$ . Dashed contours represent negative values, and solid contours represent positive values.

throughout the 4-week duration, which allows the signal to stand out from the noise in the S2S range. Strong jet extensions allow anomalously high IVT to move closer to the coast, which can force anomalously high amounts of orographically forced precipitation in California. Anomalously low precipitation along the Pacific Northwest Coast during model-observed jet extensions does not occur in regions of anomalously low IVT. This could suggest that the anomalously low precipitation associated with model-observed jet extensions is caused by ridging patterns adjacent to the synoptic eddies that allow the jet to consistently extend, which facilitates low-level divergence and suppresses convective and stratiform precipitation across the region. Such adjacent ridging patterns are shown during both jet extension regimes (Winters et al. 2019) and the positive phase of the PNA, which is also associated with a strong negative geopotential height anomaly over the central North Pacific (Wallace and Gutzler 1981). When the jet extends farther east, anticyclones are pushed farther north away from California. Based on this result, we conclude that the model-observed conditions of precipitation and IVT during strong jet extensions can dramatically vary on and near the coast depending on the existence of

conditions that enable the NPJ to be accurately forecast in the subseasonal range.

The NPJ is a source of predictability in subseasonal forecasts in the North Pacific that directly impacts IVT at the synoptic scale. Since jet extension regimes can be forecast skillfully in the subseasonal range, forecasts of wind speed in the jet exit region must hold at least some predictability. As wind is one of two components of IVT and does not have as much of a direct link to precipitation, the predictability of the NPJ favors the predictability of IVT more than it favors the predictability of precipitation. While wind patterns can lead to large-scale convergence and updrafts that can be a catalyst for precipitation, the extension of the NPJ does not have so much of a direct relationship with precipitation. For a model to generate precipitation, some of the precipitation processes will be parameterized, which could be a source of error. While >90th-percentile IVT cannot be skillfully forecast on the coast at week 4, there can still be value in predicting it to the west of the coast. The region in which IVT can be skillfully predicted intersects with the jet exit region, which is frequently an area for ARs to form, develop, and subsequently propagate toward the west coast of North America.

Since NPJ regimes can be skillfully predicted 4 weeks into the future and were closely aligned with strong IVT anomalies, processes such as anomalous tropical convection, cold surges, and persistent regimes that can lead to skillful prediction of position and strength of the NPJ likely function as potential sources of subseasonal forecast skill. Areas of persistent cyclogenesis in the North Pacific were shown to have anomalously low ensemble spread at week 4 when IVT was forecast well in the jet exit region. Additionally, there was low ensemble spread south of the anomalously high RWS activity, suggesting that conditions in the tropics are potentially a driver of subseasonal forecast skill, which has been noted in previous studies (Hoskins and Karoly 1981; Trenberth et al. 1998). Slightly downstream of the center of the negative upper-level geopotential height anomaly in the North Pacific, frequent wave activity, which is shown by the inverse Laplacian of the RWS, coincides with slightly anomalously high ensemble spread. Despite the high ensemble spread, >90th-percentile IVT conditions were still able to be predicted skillfully. The upstream anomalously high RWS that occurred near areas with low ensemble spread increased the chance in the forecast of downstream extreme conditions occurring when >90th-percentile conditions were observed. Ultimately, the predictability of high levels of IVT can serve as a useful resource to bridge the gap between skillfully predicted low frequency teleconnections in subseasonal forecasts and downstream impacts on precipitation that influence life on land.

There are some limitations to the results in this work that can provide possible opportunities for future studies. All forecasts were initialized in December, January, and February. The climatology of the NPJ varies from month to month, which could impact interactions between the predictability of IVT, precipitation, and the jet. In addition, there are limitations to assessing potential predictability. While assessing potential predictability still helps answer key questions about the possibilities of subseasonal forecasting, it does not allow us to assess prediction skill within existing weather forecasting systems. Allowing the model to be perfect eliminates model biases and errors that exist in reality. Comparing model data with reanalysis would address this limitation.

*Acknowledgments.* This work is supported by the California Department of Water Resources Ph3 Atmospheric River Research Program (Award 4600014294) and the Forecast Informed Reservoir Operations Award (USACE W912HZ1920023). The National Center for Atmospheric Research is sponsored by the National Science Foundation. The authors thank the reviewers of this work for their dedication toward supporting the research community.

*Data availability statement.* All ECMWF forecast data used for this study can be accessed from the European Centre for Medium-Range Weather Forecasts S2S database. ERA5 data can be accessed from the Copernicus Climate Data Store. ROC scores were computed using the climpred framework (<https://climpred.readthedocs.io>). North Pacific Jet forecast data can be found online (<https://scholar.colorado.edu/concern/datasets/0v838153k>).

## REFERENCES

- Ambrizzi, T., B. J. Hoskins, and H.-H. Hsu, 1995: Rossby wave propagation and teleconnection patterns in the austral winter. *J. Atmos. Sci.*, **52**, 3661–3672, [https://doi.org/10.1175/1520-0469\(1995\)052<3661:RWPATP>2.0.CO;2](https://doi.org/10.1175/1520-0469(1995)052<3661:RWPATP>2.0.CO;2).
- Amini, S., and D. M. Straus, 2019: Control of storminess over the Pacific and North America by circulation regimes: The role of large-scale dynamics in weather extremes. *Climate Dyn.*, **52**, 4749–4770, <https://doi.org/10.1007/s00382-018-4409-7>.
- Athanasiadis, P. J., J. M. Wallace, and J. J. Wettstein, 2010: Patterns of wintertime jet stream variability and their relation to the storm tracks. *J. Atmos. Sci.*, **67**, 1361–1381, <https://doi.org/10.1175/2009JAS3270.1>.
- Baggett, C. F., E. A. Barnes, E. D. Maloney, and B. D. Mundhenk, 2017: Advancing atmospheric river forecasts into subseasonal-to-seasonal time scales. *Geophys. Res. Lett.*, **44**, 7528–7536, <https://doi.org/10.1002/2017GL074434>.
- Barnston, A. G., and T. M. Smith, 1996: Specification and prediction of global surface temperature and precipitation from global SST using CCA. *J. Climate*, **9**, 2660–2697, [https://doi.org/10.1175/1520-0442\(1996\)009<2660:SAPOGS>2.0.CO;2](https://doi.org/10.1175/1520-0442(1996)009<2660:SAPOGS>2.0.CO;2).
- Brady, R. X., and A. Spring, 2021: climpred: Verification of weather and climate forecasts. *J. Open Source Software*, **6**, 2781, <https://doi.org/10.21105/joss.02781>.
- Brands, S., J. M. Gutiérrez, and D. San-Martín, 2017: Twentieth-century atmospheric river activity along the west coasts of Europe and North America: Algorithm formulation, reanalysis uncertainty and links to atmospheric circulation patterns. *Climate Dyn.*, **48**, 2771–2795, <https://doi.org/10.1007/s00382-016-3095-6>.
- Corringham, T. W., F. M. Ralph, A. Gershunov, D. R. Cayan, and C. A. Talbot, 2019: Atmospheric rivers drive flood damages in the western United States. *Sci. Adv.*, **5**, eaax4631, <https://doi.org/10.1126/sciadv.aax4631>.
- Curry, C. L., S. U. Islam, F. W. Zwiers, and S. J. Déry, 2019: Atmospheric rivers increase future flood risk in western Canada's largest Pacific river. *Geophys. Res. Lett.*, **46**, 1651–1661, <https://doi.org/10.1029/2018GL080720>.
- Dacre, H. F., P. A. Clark, O. Martínez-Alvarado, M. A. Stringer, and D. A. Lavers, 2015: How do atmospheric rivers form? *Bull. Amer. Meteor. Soc.*, **96**, 1243–1255, <https://doi.org/10.1175/BAMS-D-14-00031.1>.
- Das, T., E. P. Maurer, D. W. Pierce, M. D. Dettinger, and D. R. Cayan, 2013: Increases in flood magnitudes in California under warming climates. *J. Hydrol.*, **501**, 101–110, <https://doi.org/10.1016/j.jhydrol.2013.07.042>.
- DeFlorio, M. J., D. E. Waliser, B. Guan, F. M. Ralph, and F. Vitart, 2019a: Global evaluation of atmospheric river subseasonal prediction skill. *Climate Dyn.*, **52**, 3039–3060, <https://doi.org/10.1007/s00382-018-4309-x>.
- , and Coauthors, 2019b: Experimental Subseasonal-to-Seasonal (S2S) forecasting of atmospheric rivers over the western United States. *J. Geophys. Res. Atmos.*, **124**, 11 242–11 265, <https://doi.org/10.1029/2019JD031200>.
- Dettinger, M., 2011: Climate change, atmospheric rivers, and floods in California—A multimodel analysis of storm frequency and magnitude changes. *J. Amer. Water Resour. Assoc.*, **47**, 514–523, <https://doi.org/10.1111/j.1752-1688.2011.00546.x>.
- Fish, M. A., A. M. Wilson, and F. M. Ralph, 2019: Atmospheric river families: Definition and associated synoptic conditions. *J. Hydrometeorol.*, **20**, 2091–2108, <https://doi.org/10.1175/JHM-D-18-0217.1>.

- Franzke, C., S. B. Feldstein, and S. Lee, 2011: Synoptic analysis of the Pacific–North American teleconnection pattern. *Quart. J. Roy. Meteor. Soc.*, **137**, 329–346, <https://doi.org/10.1002/qj.768>.
- Graham, R. J., A. D. L. Evans, K. R. Mylne, M. S. J. Harrison, and K. B. Robertson, 2010: An assessment of seasonal predictability using atmospheric general circulation models. *Quart. J. Roy. Meteor. Soc.*, **126**, 2211–2240, <https://doi.org/10.1002/qj.49712656712>.
- Griffin, K. S., and J. E. Martin, 2017: Synoptic features associated with temporally coherent modes of variability of the North Pacific jet stream. *J. Climate*, **30**, 39–54, <https://doi.org/10.1175/JCLI-D-15-0833.1>.
- Guan, B., and D. E. Waliser, 2015: Detection of atmospheric rivers: Evaluation and application of an algorithm for global studies. *J. Geophys. Res. Atmos.*, **120**, 12 514–12 535, <https://doi.org/10.1002/2015JD024257>.
- Hersbach, H., and Coauthors, 2020: The ERA5 global reanalysis. *Quart. J. Roy. Meteor. Soc.*, **146**, 1999–2049, <https://doi.org/10.1002/qj.3803>.
- Higgins, R. W., J.-K. E. Schemm, W. Shi, and A. Leetmaa, 2000: Extreme precipitation events in the western United States related to tropical forcing. *J. Climate*, **13**, 793–820, [https://doi.org/10.1175/1520-0442\(2000\)013<0793:EPEITW>2.0.CO;2](https://doi.org/10.1175/1520-0442(2000)013<0793:EPEITW>2.0.CO;2).
- Hoskins, B. J., and D. J. Karoly, 1981: The steady linear response of a spherical atmosphere to thermal and orographic forcing. *J. Atmos. Sci.*, **38**, 1179–1196, [https://doi.org/10.1175/1520-0469\(1981\)038<1179:TSLROA>2.0.CO;2](https://doi.org/10.1175/1520-0469(1981)038<1179:TSLROA>2.0.CO;2).
- Jaffe, S. C., J. E. Martin, D. J. Vimont, and D. J. Lorenz, 2011: A synoptic climatology of episodic, subseasonal retractions of the Pacific jet. *J. Climate*, **24**, 2846–2860, <https://doi.org/10.1175/2010JCLI3995.1>.
- Jung, T., and M. Leutbecher, 2008: Scale-dependent verification of ensemble forecasts. *Quart. J. Roy. Meteor. Soc.*, **134**, 973–984, <https://doi.org/10.1002/qj.255>.
- Kharin, V. V., and F. W. Zwiers, 2003: On the ROC score of probability forecasts. *J. Climate*, **16**, 4145–4150, [https://doi.org/10.1175/1520-0442\(2003\)016<4145:OTRSOP>2.0.CO;2](https://doi.org/10.1175/1520-0442(2003)016<4145:OTRSOP>2.0.CO;2).
- Koster, R. D., and M. J. Suarez, 1995: Relative contributions of land and ocean processes to precipitation variability. *J. Geophys. Res.*, **100**, 13 775–13 790, <https://doi.org/10.1029/95JD00176>.
- Kumar, A., P. Peng, and M. Chen, 2014: Is there a relationship between potential and actual skill? *Mon. Wea. Rev.*, **142**, 2220–2227, <https://doi.org/10.1175/MWR-D-13-00287.1>.
- Lavers, D. A., G. Villarini, R. P. Allan, E. F. Wood, and A. J. Wade, 2012: The detection of atmospheric rivers in atmospheric reanalyses and their links to British winter floods and the large-scale climatic circulation. *J. Geophys. Res.*, **117**, D20106, <https://doi.org/10.1029/2012JD018027>.
- , F. Pappenberger, and E. Zsoter, 2014: Extending medium-range predictability of extreme hydrological events in Europe. *Nat. Commun.*, **5**, 5382, <https://doi.org/10.1038/ncomms6382>.
- , D. E. Waliser, F. M. Ralph, and M. D. Dettinger, 2016: Predictability of horizontal water vapor transport relative to precipitation: Enhancing situational awareness for forecasting western U.S. extreme precipitation and flooding. *Geophys. Res. Lett.*, **43**, 2275–2282, <https://doi.org/10.1002/2016GL067765>.
- Lorenz, E. N., 1965: A study of the predictability of a 28-variable atmospheric model. *Tellus*, **17**, 321–333, <https://doi.org/10.3402/tellusa.v17i3.9076>.
- Luo, L., and E. F. Wood, 2006: Assessing the idealized predictability of precipitation and temperature in the NCEP climate forecast system. *Geophys. Res. Lett.*, **33**, L04708, <https://doi.org/10.1029/2005GL025292>.
- Mann, M. E., and P. H. Gleick, 2015: Climate change and California drought in the 21st century. *Proc. Natl. Acad. Sci. USA*, **112**, 3858–3859, <https://doi.org/10.1073/pnas.1503667112>.
- Mariotti, A., and Coauthors, 2020: Windows of opportunity for skillful forecasts subseasonal to seasonal and beyond. *Bull. Amer. Meteor. Soc.*, **101**, E608–E625, <https://doi.org/10.1175/BAMS-D-18-0326.1>.
- Mason, S. J., and N. E. Graham, 2002: Areas beneath the Relative Operating Characteristics (ROC) and Relative Operating Levels (ROL) curves: Statistical significance and interpretation. *Quart. J. Roy. Meteor. Soc.*, **128**, 2145–2166, <https://doi.org/10.1256/003590002320603584>.
- Michaelis, A. C., A. Gershunov, A. Weyant, M. A. Fish, T. Shulgina, and F. M. Ralph, 2022: Atmospheric river precipitation enhanced by climate change: A case study of the storm that contributed to California’s Oroville Dam crisis. *Earth’s Future*, **10**, e2021EF002537, <https://doi.org/10.1029/2021EF002537>.
- Moore, B. J., A. B. White, and D. J. Gottas, 2021: Characteristics of long-duration heavy precipitation events along the West Coast of the United States. *Mon. Wea. Rev.*, **149**, 2255–2277, <https://doi.org/10.1175/MWR-D-20-0336.1>.
- Mundhenk, B. D., E. A. Barnes, and E. D. Maloney, 2016: All-season climatology and variability of atmospheric river frequencies over the North Pacific. *J. Climate*, **29**, 4885–4903, <https://doi.org/10.1175/JCLI-D-15-0655.1>.
- Neiman, P. J., F. M. Ralph, G. A. Wick, Y.-H. Kuo, T.-K. Wee, Z. Ma, G. H. Taylor, and M. D. Dettinger, 2008: Diagnosis of an intense atmospheric river impacting the Pacific Northwest: Storm summary and offshore vertical structure observed with COSMIC satellite retrievals. *Mon. Wea. Rev.*, **136**, 4398–4420, <https://doi.org/10.1175/2008MWR2550.1>.
- Palmer, T. N., 2006: Medium and extended range predictability and stability of the Pacific/North American mode. *Quart. J. Roy. Meteor. Soc.*, **114**, 691–713, <https://doi.org/10.1002/qj.49711448108>.
- Payne, A. E., and Coauthors, 2020: Responses and impacts of atmospheric rivers to climate change. *Nat. Rev. Earth Environ.*, **1**, 143–157, <https://doi.org/10.1038/s43017-020-0030-5>.
- Pendergrass, A. G., and Coauthors, 2020: Flash droughts present a new challenge for subseasonal-to-seasonal prediction. *Nat. Climate Change*, **10**, 191–199, <https://doi.org/10.1038/s41558-020-0709-0>.
- Philippon, N., F. J. Doblas-Reyes, and P. M. Ruti, 2010: Skill, reproducibility and potential predictability of the West African monsoon in coupled GCMs. *Climate Dyn.*, **35**, 53–74, <https://doi.org/10.1007/s00382-010-0856-5>.
- Prince, H. D., P. B. Gibson, M. J. DeFlorio, T. W. Corringham, A. Cobb, B. Guan, F. M. Ralph, and D. E. Waliser, 2021: Genesis locations of the costliest atmospheric rivers impacting the western United States. *Geophys. Res. Lett.*, **48**, e2021GL093947, <https://doi.org/10.1029/2021GL093947>.
- Ralph, F. M., J. J. Rutz, J. M. Cordeira, M. Dettinger, M. Anderson, D. Reynolds, L. J. Schick, and C. Smallcomb, 2019: A scale to characterize the strength and impacts of atmospheric rivers. *Bull. Amer. Meteor. Soc.*, **100**, 269–289, <https://doi.org/10.1175/BAMS-D-18-0023.1>.
- Ricciotti, J. A., and J. M. Cordeira, 2022: Summarizing relationships among landfalling atmospheric rivers, integrated water vapor transport, and California watershed precipitation 1982–2019. *J. Hydrometeorol.*, **23**, 1439–1454, <https://doi.org/10.1175/JHM-D-21-0119.1>.
- Robertson, A. W., A. Kumar, M. Peña, and F. Vitart, 2015: Improving and promoting subseasonal to seasonal prediction.

- Bull. Amer. Meteor. Soc.*, **96**, ES49–ES53, <https://doi.org/10.1175/BAMS-D-14-00139.1>.
- Sardeshmukh, P. D., and B. J. Hoskins, 1988: The generation of global rotational flow by steady idealized tropical divergence. *J. Atmos. Sci.*, **45**, 1228–1251, [https://doi.org/10.1175/1520-0469\(1988\)045<1228:TGOGRF>2.0.CO;2](https://doi.org/10.1175/1520-0469(1988)045<1228:TGOGRF>2.0.CO;2).
- Shields, C. A., and Coauthors, 2018: Atmospheric River Tracking Method Intercomparison Project (ARTMIP): Project goals and experimental design. *Geosci. Model Dev.*, **11**, 2455–2474, <https://doi.org/10.5194/gmd-11-2455-2018>.
- Stockdale, T. N., and Coauthors, 2011: ECMWF seasonal forecast system 3 and its prediction of sea surface temperature. *Climate Dyn.*, **37**, 455–471, <https://doi.org/10.1007/s00382-010-0947-3>.
- Trenberth, K. E., G. W. Branstator, D. Karoly, A. Kumar, N.-C. Lau, and C. Ropelewski, 1998: Progress during TOGA in understanding and modeling global teleconnections associated with tropical sea surface temperatures. *J. Geophys. Res.*, **103**, 14 291–14 324, <https://doi.org/10.1029/97JC01444>.
- Vitart, F., and Coauthors, 2017: The Subseasonal to Seasonal (S2S) prediction project database. *Bull. Amer. Meteor. Soc.*, **98**, 163–173, <https://doi.org/10.1175/BAMS-D-16-0017.1>.
- Waliser, D., and B. Guan, 2017: Extreme winds and precipitation during landfall of atmospheric rivers. *Nat. Geosci.*, **10**, 179–183, <https://doi.org/10.1038/ngeo2894>.
- Wallace, J. M., and D. S. Gutzler, 1981: Teleconnections in the geopotential height field during the Northern Hemisphere winter. *Mon. Wea. Rev.*, **109**, 784–812, [https://doi.org/10.1175/1520-0493\(1981\)109<0784:TITGHF>2.0.CO;2](https://doi.org/10.1175/1520-0493(1981)109<0784:TITGHF>2.0.CO;2).
- White, C. J., and Coauthors, 2017: Potential applications of Subseasonal-to-Seasonal (S2S) predictions. *Meteor. Appl.*, **24**, 315–325, <https://doi.org/10.1002/met.1654>.
- , and Coauthors, 2022: Advances in the application and utility of subseasonal-to-seasonal predictions. *Bull. Amer. Meteor. Soc.*, **103**, E1448–E1472, <https://doi.org/10.1175/BAMS-D-20-0224.1>.
- Williams, A. P., R. Seager, J. T. Abatzoglou, B. I. Cook, J. E. Smerdon, and E. R. Cook, 2015: Contribution of anthropogenic warming to California drought during 2012–2014. *Geophys. Res. Lett.*, **42**, 6819–6828, <https://doi.org/10.1002/2015GL064924>.
- Winters, A. C., 2021: Subseasonal prediction of the state and evolution of the North Pacific jet stream. *J. Geophys. Res. Atmos.*, **126**, e2021JD035094, <https://doi.org/10.1029/2021JD035094>.
- , D. Keyser, and L. F. Bosart, 2019: The development of the North Pacific jet phase diagram as an objective tool to monitor the state and forecast skill of the upper-tropospheric flow pattern. *Wea. Forecasting*, **34**, 199–219, <https://doi.org/10.1175/WAF-D-18-0106.1>.
- Zhang, Z., F. M. Ralph, and M. Zheng, 2019: The relationship between extratropical cyclone strength and atmospheric river intensity and position. *Geophys. Res. Lett.*, **46**, 1814–1823, <https://doi.org/10.1029/2018GL079071>.